Effects of surface micromesas on reverse leakage current in InGaN/GaN Schottky barriers

Wei Lu,[1,a)] Tomoaki Nishimura,[2] Lingquan (Dennis) Wang,[1] Tohru Nakamura,[3] Paul K. L. Yu,[1] and Peter M. Asbeck[1]
[1]*Department of Electrical and Computer Engineering, University of California, San Diego, La Jolla, California 92093, USA*
[2]*Research Center of Ion Beam Technology, Hosei University, Tokyo 184-8584, Japan*
[3]*Department of Electrical and Electronics Engineering, Hosei University, Tokyo 184-8584, Japan*

(Received 26 March 2012; accepted 25 July 2012; published online 23 August 2012)

This work shows the correlation between excess reverse leakage currents in InGaN/GaN Schottky barrier diodes and the presence of surface micromesas on these structures. Surface micromesas with diameters of 1–2 μm and density in the range of $10^5\,cm^{-2}$ were observed in metal-organic-chemical-vapor-deposition-grown InGaN ($\sim$10 nm)/GaN epi-layers on c-sapphire substrates. Nomarski optical microscopy, scanning electron microscopy, and atomic force microscopy were used to investigate characteristics of the surface micromesas. We found that most of the surface micromesas originated from nanopipes in GaN as they intersected the InGaN/GaN epi-layer surface. Extensive current-voltage and Rutherford backscattering spectrometry measurements on the corresponding Ni-InGaN/GaN Schottky barriers revealed that these surface micromesas with nanopipes at their center were likely the main source of reverse leakage current. They also provide an easy metal diffusion path when devices undergo thermal annealing, even at relatively low temperatures. High-pressure (near atmospheric pressure) buffer layer growth can be used to minimize the surface micromesas and the leakage currents. © *2012 American Institute of Physics*. [http://dx.doi.org/10.1063/1.4748317]

I. INTRODUCTION

III-nitride heterostructures have been widely implemented in both electronic and opto-electronic device applications. The development of III-nitride heterostructure growth techniques and the unique property of polarization charges at the heterojunction interface provide great convenience and flexibility in device design. InGaN/GaN, as one of the prevalent III-nitride heterostructure combinations, has attracted intense interest in relation to light emitting diodes (LEDs),[1,2] heterojunction bipolar transistors (HBTs),[3,4] and high power electronic devices.[5,6] However, due to the large lattice mismatch and thermal expansion mismatch to the substrates, epi-grown nitride materials suffer from a variety of defects, such as threading dislocations (TDs), stacking faults, inversion domain boundaries, and nanopipes.[7,8] Although not all defects are detrimental to device performance since long-lived LEDs and lasers can be fabricated on nitride materials even with $10^8\,cm^{-2}$ dislocation density, the effects of these defects on device characteristics are still topics of considerable interest. This work addresses the relationship between dislocations and surface micromesas in the InGaN/GaN system and shows that micromesas are associated with excess leakage currents in InGaN/GaN Schottky barrier diodes, especially at higher annealing temperatures.

Previous work has elucidated many of the characteristics of GaN and InGaN defects. Nanopipes, with radii of 35 to 500 Å, in metal-organic-chemical-vapor-deposition (MOCVD)-grown GaN epi-layers were first reported by Qian *et al.*[8] Their scanning force microscopy (SFM) and high-resolution transmission electron microscopy (TEM) studies revealed that the nanopipes are open cores of screw TDs.[9] These hollow pipes were predicted earlier by Frank, who noted that for a dislocation whose Burgers vector exceeds a critical value, there exists a local equilibrium state in which the dislocation core is an empty tube.[10] Similar defects, named micropipes (with sizes more than two orders of magnitude larger than those of the nanopipes observed in GaN), are frequently observed in SiC, another wide bandgap semiconductor with hexagonal crystal structure.[11,12] The micropipes in SiC can be observed by optical microscopy and have been reported to be detrimental to the performance of devices. Neudeck *et al.* reported that micropipes are the main source of electrical breakdowns in SiC p-n junction diodes and limiting factors for applications of SiC in high-power, high-frequency, and high-temperature electronic devices.[13,14] In contrast to the micropipes in SiC, the nanopipes in GaN cannot be observed by optical microscopy because of their small sizes; usually TEM or wet chemical etching techniques are required to observe them.[9,15,16] Therefore, it is difficult to study the direct correlation between the nanopipes and the electrical characteristics of the nitride devices.

In this work, we investigated the surface defects in MOCVD-grown InGaN/GaN materials by Nomarski optical microscopy (NOM), scanning electron microscopy (SEM), and atomic force microscopy (AFM). Different growth pressures for GaN buffer layers were used to vary the material defect density.[17,18] After adding a thin surface layer of InGaN, micro-scale surface mesas were observed by NOM. We were able to use a large-scale defect mapping method before and after hot

a)Electronic mail: w8lu@ucsd.edu.

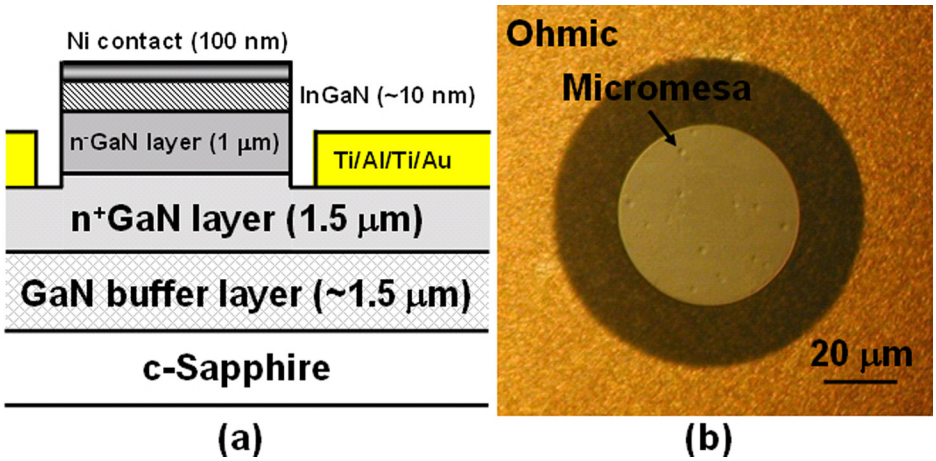

FIG. 1. (a) Schematic cross section of the InGaN/GaN Schottky diode and (b) the Nomarski optical microscopy top view of a real diode with surface micromesas.

phosphoric acid (H_3PO_4) etching to analyze the origin of the surface micromesas and relate them to nanopipes. Direct NOM observation of the micromesas allowed us to study the effects of micromesas, and by inference, nanopipes, on reverse leakage current in Ni-InGaN/GaN Schottky barriers. Detailed surface topography of micromesas was investigated by SEM and AFM. We previously reported the breakdown characteristics improvement of GaN Schottky diodes by adding a thin InGaN surface layer.[5,18] Here we further study the reverse leakage current in InGaN/GaN Schottky barriers with extensive measurements of reverse leakage current versus diode dimension and micromesa number before and after thermal annealing at different temperatures. We show an increase of leakage current with thermal annealing, which is sometimes an essential step in device fabrication (e.g., thermally curing polymers for metal isolation). Rutherford backscattering spectrometry (RBS) measurements are also used to study the inter-diffusion between Ni and InGaN/GaN at different annealing temperatures. We conclude that the micromesas are the main source of leakage in these structures. We show that high pressure epitaxial growth can significantly reduce micromesa density and thus leakage current.

II. EPITAXIAL GROWTH PROCEDURES

The structure of the Schottky barrier diodes investigated in this work is shown in Fig. 1(a). The epitaxial structure is chosen to minimize leakage currents and avoid diode breakdown, with high applied reverse voltages. The materials were processed into circular mesa diodes of the form illustrated in Fig. 1(b). The Nomarski micrograph of the diode illustrated shows the presence of surface micromesas.

All samples used in this study were grown using a Thomas Swan close-coupled showerhead $3 \times 2''$ MOCVD system. Two-inch diameter wafers of c-sapphire were used as substrate material. We used the traditional low temperature (LT) GaN nucleation layer method for the material growth, followed by high temperature (HT) GaN buffer layer growth.[19] Subsequently a 1.5-μm HT n^+ GaN ($n \approx 5 \times 10^{18}\,cm^{-3}$) layer and a 1-$\mu$m HT n^- GaN ($n \approx 1 \times 10^{17}\,cm^{-3}$) layer were grown. Four wafers were grown as part of this study. Growth details and sample labels are summarized in Table I. Low pressure (LP) growths utilized 300 mbar pressure for the buffer layer growth, while high pressure (HP) samples employed 900 mbar in this step. The HP (near atmosphere pressure) buffer layer growth was found to reduce the defect density.[17,18] For HP_InGaN/GaN and LP_InGaN/GaN samples, there were ~10-nm InGaN surface layers grown on top. After the MOCVD growth, the wafers were diced into 1×1 cm^2 squares for various experiments.

III. MATERIAL CHARACTERIZATION

A. X-ray diffraction measurements

Full width at half maximum (FWHM) of symmetric (0002) and asymmetric ($10\bar{1}2$) x-ray rocking curves (XRCs) were measured to compare the threading dislocation densities in these four samples. The results are included in Table II. It is known that the FWHM of the symmetric (0002) XRC is broadened by screw- and mixed-type threading dislocations and the asymmetric ($10\bar{1}2$) XRC is broadened by all TDs.[20,21] Narrower FWHM of the samples (HP_GaN and HP_InGaN/GaN) using higher growth pressure for GaN

TABLE I. Sample labels and key growth details used in this work (the coalescence time for HP buffer and LP buffer is ~50 min and ~10 min, respectively; the growth rate for HP buffer an LP buffer is ~0.52 nm/s and ~0.46 nm/s, respectively; and the InGaN growth rate is ~0.0326 nm/s).

Sample label	LP_GaN	LP_InGaN/GaN	HP_GaN	HP_InGaN/GaN
InGaN layer	N.A.	~6% In, ~10 nm, 400 mbar, 808 °C	N.A.	~6% In, ~10 nm, 400 mbar, 808 °C
Common layers	n^- GaN ($n \approx 1 \times 10^{17}\,cm^{-3}$, 1 μm), 200 mbar, 1040 °C			
	n^+ GaN ($n \approx 5 \times 10^{18}\,cm^{-3}$, 1.5 μm), 200 mbar, 1040 °C			
	GaN buffer (~1.5 μm), 300 mbar for low pressure (LP), 900 mbar for high pressure (HP) GaN buffer, 1040 °C			
	Low-temperature GaN nucleation layer (~20 nm), 600 mbar, 530 °C			
	c-Sapphire substrate			

TABLE II. FWHM of symmetric (0002) and asymmetric ($10\bar{1}2$) XRCs, surface micromesa density estimated under Nomarski optical microscopy and nanopipe and TD densities estimated by EPD in all samples.

Sample label	FWHM of (0002)/($10\bar{1}2$) XRCs (arc sec)	Micromesa density by NOM (before etch) (cm^{-2})	Nanopipe density by EPD (cm^{-2})	TD density by EPD from AFM (cm^{-2})
HP_InGaN/GaN	276/325	1.6×10^5	1.9×10^5	1.5×10^8
LP_InGaN/GaN	347/476	5.8×10^5	6.8×10^5	2.8×10^8
HP_GaN	281/334	0	2.5×10^5	1.6×10^8
LP_GaN	338/440	0	9.1×10^5	3.0×10^8

buffer layers indicates lower edge-, screw- and mixed-type TD densities than those of the samples (LP_GaN and LP_InGaN/GaN) using low pressure growth for GaN buffer layers.

B. Nomarski microscopy imaging

Smooth surfaces are observed for the GaN-only (LP_GaN and HP_GaN) samples, while large surface mesas, with density in the range of $10^5\,cm^{-2}$, are optically observable on the LP_InGaN/GaN and HP_InGaN/GaN samples as shown in Fig. 2 with only ~10-nm InGaN top layers. These surface mesas are typically 1–2 μm in diameter and less than 30 nm in height on our ~10-nm InGaN containing samples from NOM and AFM measurements. Corresponding with lower TD density estimated by XRC measurements, the InGaN/GaN sample grown using higher growth pressure for the GaN buffer layer also shows a much lower surface micromesa density as shown in Table II.

C. Surface topography investigation by SEM and AFM

Representative SEM and AFM micrographs of the surface micromesas on InGaN/GaN samples are shown in Fig. 3. The micromesa shows spiral steps, which typically emerge from a nanopipe. By carefully examining the height of the different resolvable steps showing in Fig. 3(b), the step heights were found to be around several nanometers, roughly with a greatest common divisor (GCD) of 5.4 ± 0.3 Å. This GCD is consistent with the expected value of c-lattice constant of InGaN (5.19 Å and 5.69 Å for GaN and InN, respectively).[22] The measured step heights that are integer multiples (typically 2–4) of the GCD (~c-lattice constant of InGaN) are consistent with the step sizes reported for growth spirals in other material systems, and can be attributed to step bunching.[23]

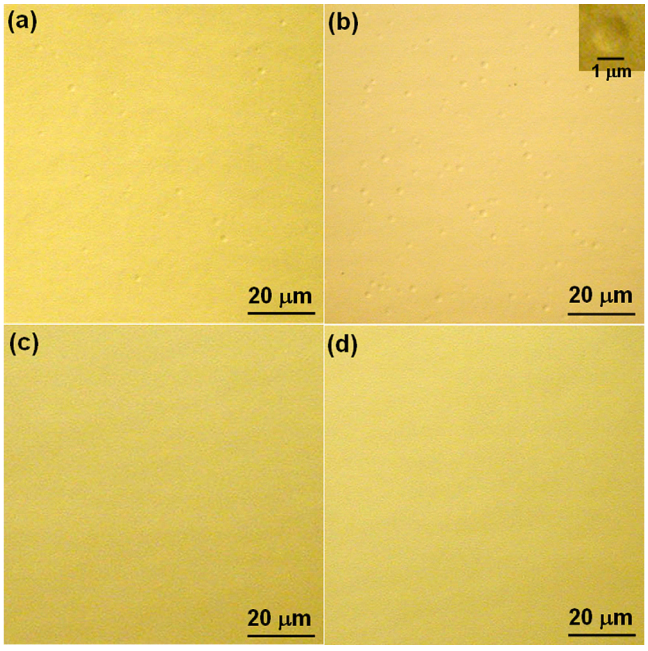

FIG. 2. Nomarski optical microscopy images of (a) HP_InGaN/GaN, (b) LP_InGaN/GaN, (c) HP_GaN, and (d) LP_GaN. The inset in (b) is a zoom-in image of one surface micromesa.

D. Etch pit density measurements

All samples were immersed into 180 °C H_3PO_4 for 7 min to perform the etch pit density (EPD) measurements[24] and followed by NOM, SEM, and AFM investigations to analyze the etch pit type and density. Fig. 4 shows the AFM images of the etched HP_InGaN/GaN and LP_InGaN/GaN samples and their corresponding surface profiles. The TD densities in the range of $10^8\,cm^{-2}$ in these samples can be estimated by counting the etch pits in these images.

Although the SEM and AFM micrographs in Fig. 3 show that the surface micromesas grow spirally around the nanopipes, the scanning areas for these two techniques are too small to conclusively identify the origin of the surface micromesas. Therefore, for the LP_InGaN/GaN sample, surface micromesas (before etch) and etch pits were mapped using NOM over a large area for further characterization. For better comparison, two representative small parts of the zoomed-in mapped images are shown in Fig. 5. The small etch pits that correspond to the TDs shown in the AFM images cannot be observed by NOM. The observable etch pits (black dots) under the NOM shown in Fig. 5(b) represent the same type of defect as the large etch pit shown in the AFM image in Fig. 4(c) (indicated by an arrow), which is clearly different from the other small TD-related etch pits in the AFM images. These large etch pits have a density in the range of $10^5\,cm^{-2}$, which is three orders of magnitude lower than the TD density.

E. Discussion of material defect characterization

Hong *et al.* performed thorough TEM studies of the origin of the hexagonal-shaped etch pits in (0001) GaN films and concluded that these etch pits with a density 2–4 orders of magnitude lower than the TD density originated from

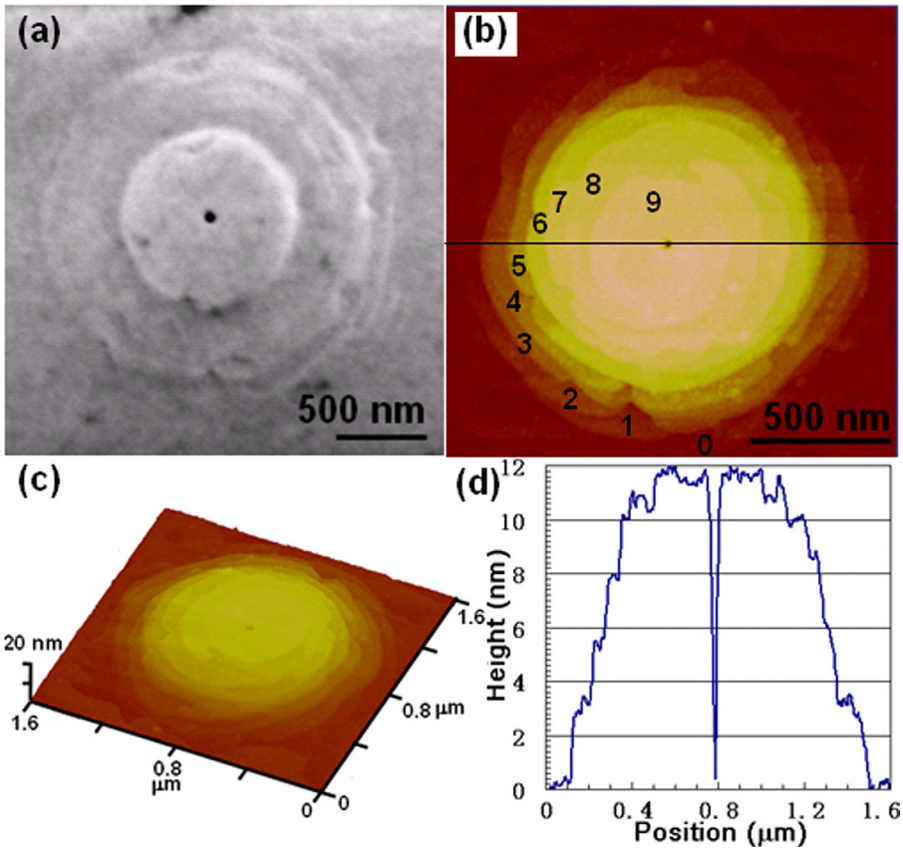

FIG. 3. Representative SEM and AFM (tapping mode) micrographs of the surface micromesas. (a) A SEM micrograph; (b) an AFM micrograph; (c) 3-D AFM micrograph of (b); and (d) surface profile along the line shown in (b). (b)-(d) are from the same micromesa and (a) is from a different one. Numbers in (b) indicate the resolvable spiral steps.

nanopipes (open-core screw TDs).[15,25] The $10^5\,cm^{-2}$ EPD that was measured is also quite close to those reported nanopipe densities in MOCVD-grown GaN films.[8,9] Based on our consistent observations with their TEM studies, we believe that the large etch pits in the AFM and NOM images originate from nanopipes.

Furthermore, from the mapping images shown in Fig. 5, it can be clearly seen that most of the surface micromesas

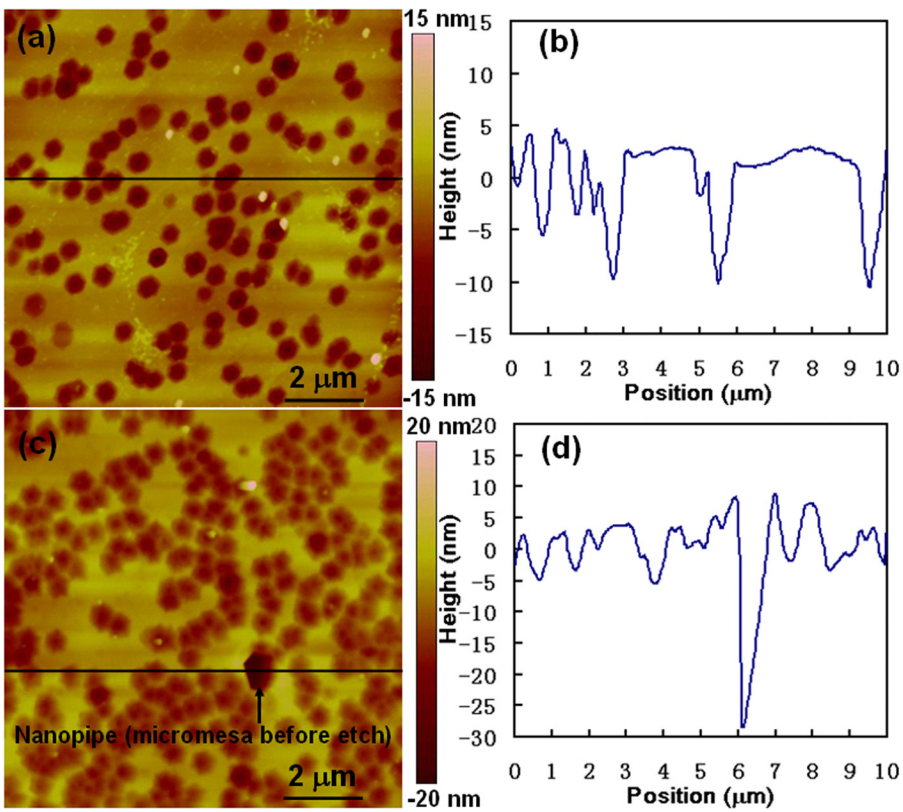

FIG. 4. $10 \times 10\,\mu m^2$ AFM images of (a) HP_InGaN/GaN, (b) surface profile along the line in (a), (c) LP_InGaN/GaN, and (d) surface profile along the line in (c) after H_3PO_4 etch.

(~80%) form nanopipe-related etch pits. This is consistent with the micromesa observations under SEM and AFM shown in Fig. 3. In accordance with the aforementioned TEM studies, the hexagonal-shaped etch pit shown in the inset of Fig. 5(b) is formed by etching along the nanopipe at the center of the micromesa shown in Fig. 3. Indium incorporation at lower growth temperatures is considered an important factor in the formation of surface micromesas, since no surface micromesas were observed on the GaN-only samples. Indium atoms have much higher surface mobility on the GaN surface than Ga atoms at the lower InGaN growth temperature, giving them higher probability to occupy the lowest energy sites and form spiral steps around the nanopipes.[26,27] The roughly extracted c-lattice constant value of 5.4 ± 0.3 Å from the AFM micrograph of the surface micromesa also suggests a high indium concentration in the micromesa area. The indium segregation around nanopipes (open-core screw TDs) has also been observed by energy dispersive x-ray (EDX) measurements in InAlN/GaN systems.[28] Therefore, we may speculate that the surface micromesa is formed by indium-rich spiral growth around nanopipes at lower InGaN growth temperatures with a growth rate that is higher than that of the planar growth on the remaining GaN surface.

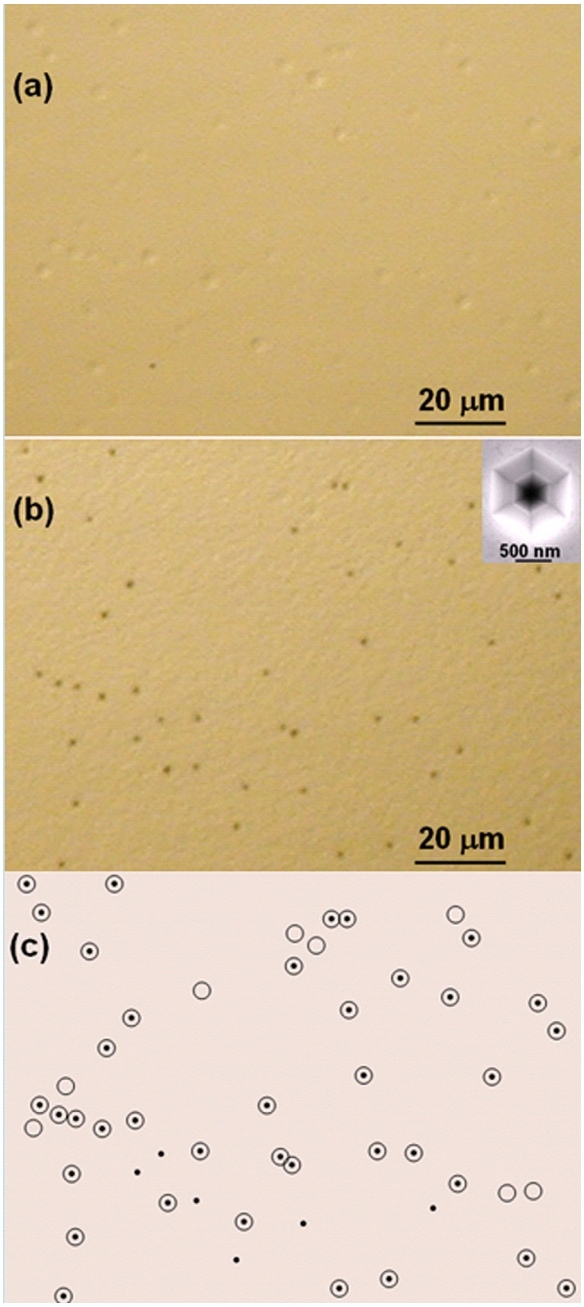

FIG. 5. Surface micromesa mapping by Nomarski optical microscopy. (a) Surface micromesas before etch and (b) etch pits in the same area of a LP_InGaN/GaN sample. (c) A schematic superposition of image (a) and (b). The inset in (b) is a representative SEM image of a large etch pit shown in (b). The circles and dots in (c) represent the surface micromesas and nanopipe-related etch pits, respectively.

As shown schematically in Fig. 5(c) with the superposition of the two mapping images, some surface micromesas that do not form nanopipe-related etch pits and some nanopipe-related etch pits that do not correspond to optically observable micromesas were also observed. Fig. 6 shows corresponding micrographs of the surface micromesas (with and without nanopipes at the center) and a nanopipe (without formation of a surface micromesa) that were found consistent with the observations in the mapping images in Fig. 5(c). The former case could be attributable to the formation of surface micromesas around some defect other than a nanopipe, e.g., stacking fault within the InGaN layer due to strain relaxation;[29] the latter case could be due to inhibition of spiral growth around nanopipes due to the local strain in the InGaN layer. These tentative explanations, however, need to be further investigated.

Table II summarizes the results of XRC measurements and surface micromesa and TD densities for the four samples. The surface micromesa, nanopipe, and TD densities in HP_GaN and HP_InGaN/GaN samples are lower as expected, which is consistent with their narrower FWHM of XRCs. In the InGaN/GaN samples, the surface micromesa density of $\sim 10^5\,\mathrm{cm}^{-2}$ is close to the nanopipe density and much lower than the TD density of $\sim 10^8\,\mathrm{cm}^{-2}$. This is also a good indication that the surface micromesas have a close relationship with nanopipes but little relationship with other

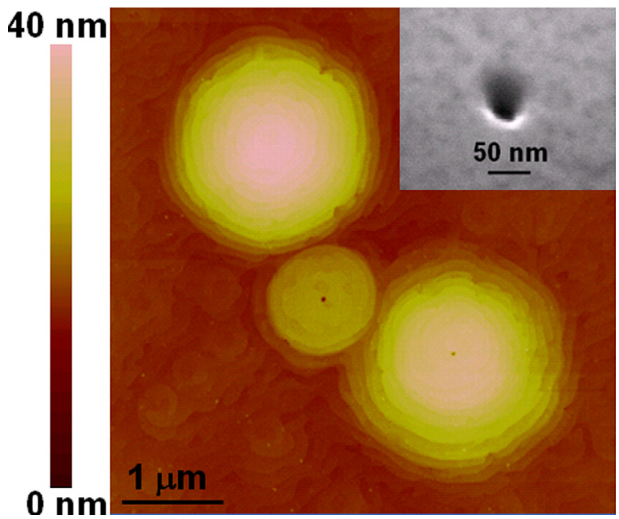

FIG. 6. An AFM (tapping mode) micrograph of surface micromesas with and without nanopipes at the center. The inset is a SEM image of a nanopipe without formation of a surface micromesa on the InGaN/GaN sample.

TDs. In addition, the reduction of nanopipe-related EPD by adding a thin InGaN surface layer ($9.1 \times 10^5\,cm^{-2}$ to $6.8 \times 10^5\,cm^{-2}$ between LP_GaN and LP_InGaN/GaN, and $2.5 \times 10^5\,cm^{-2}$ to $1.9 \times 10^5\,cm^{-2}$ between HP_GaN and HP_InGaN/GaN, respectively) is significant. However, the additional InGaN surface layer does not introduce too much TD density change. This observation is in agreement with the work of Ono *et al.*[16]

IV. DIODE FABRICATION AND ELECTRICAL CHARACTERISTICS

HP_InGaN/GaN and LP_InGaN/GaN samples were fabricated into Schottky diodes to investigate their electrical characteristics. Samples were first cleaned using organic solvent and then immersed in NH_4OH for 1 min to remove the native carbon and oxide contaminations right before the ~100-nm Ni Schottky contact deposition. The Ni and InGaN/GaN layers were then patterned and etched to form mesa diodes with different diameters in the range of 17 μm to 280 μm. 0.1-mol/L KOH treatment was used to reduce the InGaN/GaN dry-etch residuals and then a Ti/Al/Ti/Au (20 nm/80 nm/50 nm/100 nm) metal stack was used as the ohmic contact on the n^+ GaN, as illustrated in Fig. 1.

The IV characteristics were measured on different sizes of diodes. The relation between leakage current at a reverse bias (V_r) of 30 V and diode diameter is shown in Fig. 7. The data trend which follows the slope-of-two line (except for the smallest HP_InGaN/GaN diodes) on a logarithmic scale indicates that the leakage current is proportional to the corresponding area of the diodes, instead of being dominated by edge effects. The HP_InGaN/GaN Schottky diodes with lower surface micromesa and nanopipe density showed about two orders of magnitude lower leakage current than that of LP_InGaN/GaN diodes. From the estimated micromesa density shown in Table II, the average area per micromesa is 625 μm^2 for HP_InGaN/GaN and 172 μm^2 for LP_InGaN/GaN, which in turn correspond to critical diameters D_c of 28 μm and 15 μm, respectively. Diodes without micromesas are expected to occur (on a probabilistic basis) when diode diameter becomes close to or smaller than D_c. As seen from Fig. 7, the smallest LP_InGaN/GaN Schottky diodes with diameters of 17 μm (close to the value of D_c for this wafer of 15 μm), showed large scattering of leakage currents around their slope-of-two trend; the smallest HP_InGaN/GaN Schottky diodes with diameters of 17 μm (much smaller than the value D_c of for this wafer, 28 μm) showed significantly lower leakage current than their slope-of-two trend. This suggests that the micromesas are likely a major leakage path in the InGaN/GaN Schottky diodes.

To confirm the relationship, the number of micromesas for each of the smallest (17-μm diameter) Ni-InGaN/GaN Schottky diodes was first counted under NOM, and then a study of their forward and reverse IV characteristics was performed. Fig. 8 shows the relation between leakage current at $V_r = 30$ V and micromesa number on the smallest diodes. It is clear that the leakage current increases with the increase of micromesa number. Representative forward IV curves for the smallest diodes without and with surface micromesas are shown in Fig. 9. In Fig. 9(a), the IV curve for the diode without surface micromesa has an ideality factor of ~1.3, which is larger than unity due to the polarization charge (at the InGaN/GaN interface)-induced Schottky barrier height (SBH) increase as forward bias increases.[18] The corresponding calculations based on thermionic emission (TE) theory fit the experimental curve well.[18] In Fig. 9(b), IV curves with two distinctive turn-on mechanisms were usually observed for the diodes with surface micromesas. The first turn-on mechanism in the low bias region can be modeled as due to the surface micromesa with lower SBH and higher series resistance (R_s) (due to its small area); the second turn-on mechanism, associated with the high bias region, originates from the normal InGaN/GaN Schottky barrier, with higher SBH and lower R_s. A schematic equivalent circuit diagram for explaining this two turn-on phenomenon was also proposed in the Fig. 9(b). In the TE-based calculations,[18] using effective SBHs of micromesas 0.3–0.5 eV lower than effective SBHs of Ni-InGaN/GaN (~1.1 eV), and R_s of micromesa around two orders of magnitude larger (due to <1% micromesa area) than R_s of Ni-InGaN/GaN can match the experimental curves quite well. The lower effective SBH is

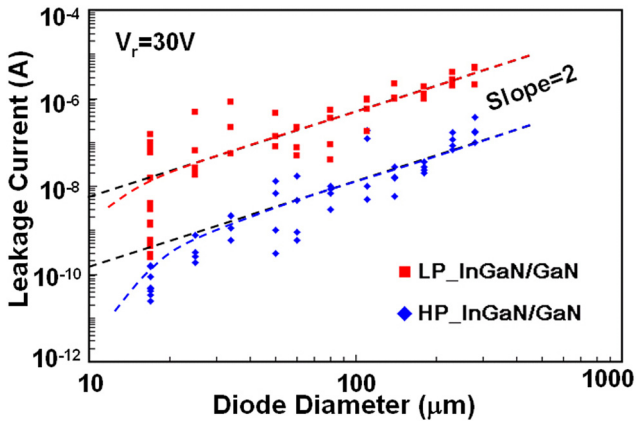

FIG. 7. Leakage current at a reverse bias of 30 V versus diode diameter for LP_InGaN/GaN and HP_InGaN/GaN Schottky diodes. The black dashed lines have slope of two and the color dashed curves represent the trend of measured data points.

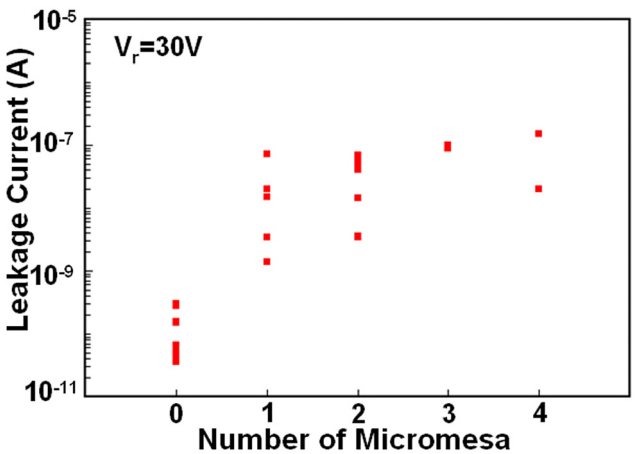

FIG. 8. Leakage current at a reverse bias of 30 V versus micromesa number on the smallest (17-μm diameter) LP_InGaN/GaN and HP_InGaN/GaN Schottky diodes.

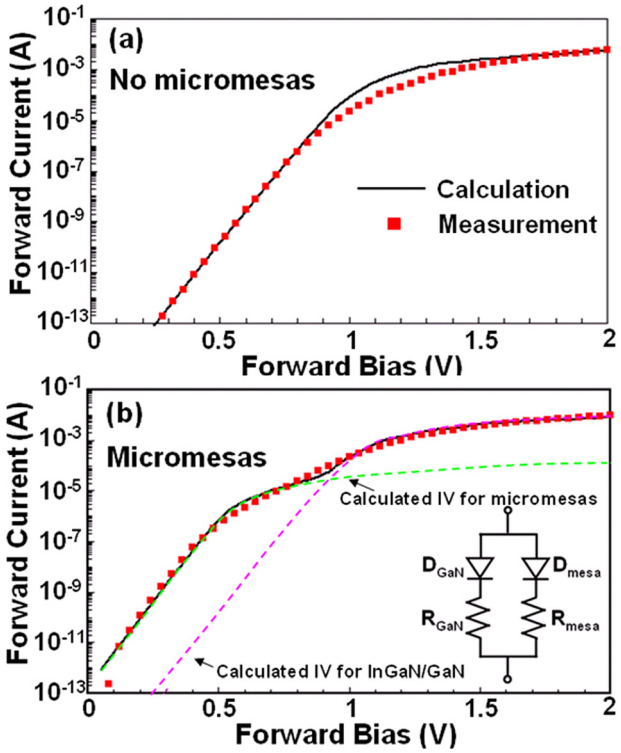

FIG. 9. Representative forward IV curves for the smallest (17-μm diameter) Ni-InGaN/GaN Schottky barriers (a) without surface micromesas and (b) with surface micromesas. The red dots are measured data and the solid black curves are calculated thermionic emission (TE) currents. In (b), the green and pink dashed curves represent the calculated TE currents for micromesas and InGaN/GaN, respectively. The black solid curve is the summation of the two dashed curves. The inset is the equivalent circuit diagram of the InGaN/GaN Schottky diodes with surface micromesas.

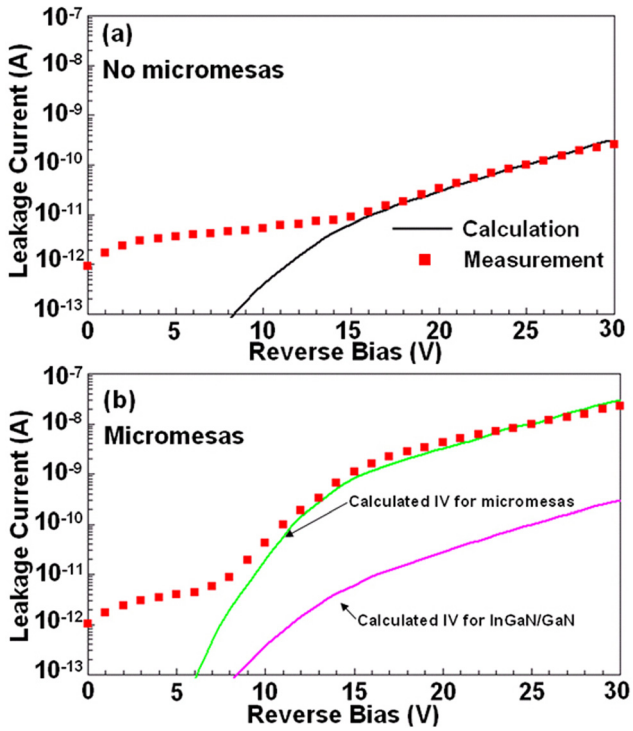

FIG. 10. Representative reverse-bias IV curves for the smallest (17-μm diameter) Ni-InGaN/GaN Schottky barriers (a) without surface micromesas and (b) with surface micromesas. The red dots are measurement data and the solid curves are calculated tunneling currents. In (b), the green curve is calculated tunneling current for micromesas and the pink curve is calculated tunneling current for InGaN/GaN.

likely caused by the lower conduction band edge (E_c) of InGaN and partial strain relaxation at the InGaN/GaN interface due to higher indium concentration and larger InGaN layer thickness (estimated by AFM) in the micromesa area.

Representative reverse-bias IV curves and the corresponding calculated curves for the smallest InGaN/GaN Schottky diodes are shown in Fig. 10. The calculations based on electron tunneling through the Schottky barrier under reverse biases fit the experimental curves well in the high-bias regime.[18] In the low-bias regime, the tunneling current is much lower than the equipment noise current and is difficult to measure. In Fig. 10(b), it is clearly seen that when miocromesas exist, the micromesas with effective SBHs 0.3–0.5 eV lower than that of InGaN/GaN were the main source of the leakage current even though they only occupy $\sim$ <1% area of the diode. The values of the key parameters used for all calculations in this work are summarized in Table III.

V. EFFECTS OF THERMAL ANNEALING

The InGaN/GaN Schottky-diode samples were annealed in forming gas (5% H_2 in N_2) at different temperatures to study the effects of thermal annealing on reverse leakage current. In parallel, InGaN/GaN samples covered with $\sim$100-nm Ni films were also annealed in order to study the Ni diffusion at the Ni/InGaN interface using RBS measurements. RBS measurements were carried out using 1.5 MeV $^4He^+$ ions with a scattering angle of 150°. As shown in the measured RBS spectra in Fig. 11, for annealing at 200 °C for 60 min no diffusion was detected from RBS measurements;

TABLE III. Values of the key parameters used for all calculations in this work (the other parameters used in the calculations but not listed here are all theoretical physical constants, e.g., q, k, etc.).

N_d (n^- GaN)	$1.0–1.1 \times 10^{17}$ cm^{-3}	t (InGaN)	10–13 nm	ϕ_{b0} (InGaN/GaN)	0.9 eV[d]
N_d (InGaN)	$4–5 \times 10^{17}$ cm^{-3}[a]	σ ($In_{0.06}Ga_{0.94}N$)	$1.7–2.0 \times 10^{12}$ cm^{-2}[c]	ϕ_{b0} (micromesa)	0.4–0.6 eV[d]
ε_{GaN}	$8.9 \times \varepsilon_0$[b]	ΔE_c ($In_{0.06}Ga_{0.94}N$)	0.09 eV (Ref. 30)	R_s (InGaN/GaN)	50–100 Ω
$\varepsilon_{In0.06Ga0.94N}$	$9.28 \times \varepsilon_0$[b]	A (diode area)	2.25×10^{-6} cm^2	R_s (micromesa)	5000–10 000 Ω

[a]The unintentionally doped InGaN is expected to be n-type doped (Ref. 31).
[b]$\varepsilon_0 = 8.85 \times 10^{-14}$ F/cm is the dielectric constant of vacuum. $\varepsilon_{InxGa1-xN}$ is linearly interpolated values from $\varepsilon_{GaN} = 8.9 \times \varepsilon_0$ and $\varepsilon_{InN} = 15.3 \times \varepsilon_0$ (Ref. 22).
[c]Estimated values by *C-V* measurements (Ref. 18).
[d]ϕ_{b0} is the Schottky barrier height defined by the difference between the Ni work function and the InGaN conduction band edge. The effective Schottky barrier height, which is calculated by taking the polarization charges into consideration, is higher than ϕ_{b0} (Ref. 18).

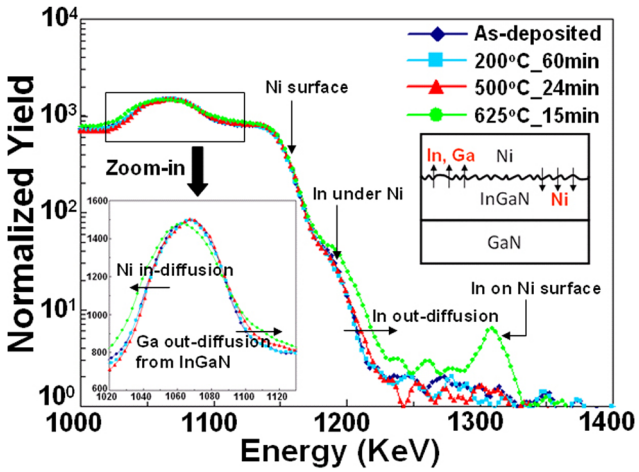

FIG. 11. RBS spectra of as-deposited, annealed at 200 °C for 60 min, 500 °C for 24 min, and 625 °C for 15 min Ni-InGaN/GaN samples. The inset on the left shows the zoom-in spectra and the inset on the right is a schematic diagram of the inter-diffusion at the Ni-InGaN interface.

for annealing at 500 °C for 24 min, weak Ga and In out-diffusion were observed; for annealing at 625 °C for 15 min, extensive Ga and In out-diffusion and Ni in-diffusion were observed.

The relation between leakage current at $V_r = 30$ V and the diode diameter before and after annealing at 200 °C for 1 h and 500 °C for 24 min is shown in Fig. 12. After 1-h annealing at 200 °C, leakage current increase was significant for large-size diodes. However, the small-size diodes did not show significant leakage current increase. More data points were measured for the smallest diodes. It is seen that for the smallest HP_InGaN/GaN diodes with diameters of 17 μm much smaller than their D_c of 28 μm showed little leakage current degradation after 200 °C annealing. Although the RBS measurement did not detect any diffusion at 200 °C annealing, the results of leakage current versus diameter (reverse leakage degradation only observed for larger diodes that contain surface micromesas) suggest that the surface micromesas with nanopipes at their center were likely an easy diffusion path at lower temperatures (e.g., 200 °C). This

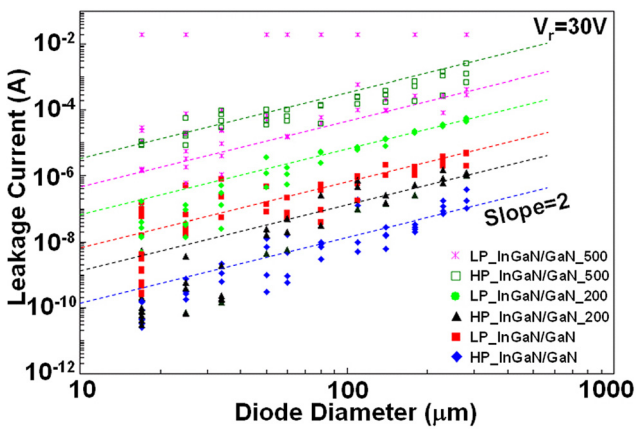

FIG. 12. Leakage current at a reverse bias of 30 V versus diode diameter for LP_InGaN/GaN and HP_InGaN/GaN Schottky diodes before and after annealing at different temperatures.

diffusion, however, is difficult to measure by RBS due to <1% diode area for the surface micromesas. Diffusion through surface micromesas would degrade the Schottky barriers, so the smallest diodes without surface micromesas would not be affected by the 200 °C annealing. This was confirmed by experimental data. Similar metal diffusion through the cores of TDs in GaN-based LEDs was already observed at higher temperatures (>600 °C) under TEM by Hsu *et al.*[32] The reverse-bias IV curves can be also fitted using tunneling current calculations (not shown) by lowering the SBH of micromesas by ~0.07 eV from the SBH value used before annealing.

After 24-min annealing at 500 °C, all diodes showed significant leakage current increase and some LP_InGaN/GaN diodes suffered breakdown at $V_r < 30$ V. This suggests that extensive diffusion started at the Ni/InGaN interface and degraded the Ni-InGaN/GaN Schottky barriers (leading to ~0.25 eV SBH lowering relative to the SBH value used before annealing according to the tunneling current calculations). This is also consistent with our RBS measurements.

VI. CONCLUSIONS

Surface micromesas were observed on InGaN/GaN epilayers, and their characteristics and origin were investigated by NOM, SEM, and AFM. Large-scale mapping between surface micromesas and etch pits under NOM revealed that most of the surface micromesas originated from nanopipes in GaN. Studies of RBS and the electrical characteristics on corresponding Ni-InGaN/GaN Schottky barriers indicated that the surface micromesas with nanopipes at the center were the main source of reverse leakage current and caused an easy metal diffusion path, even in relatively low-temperature thermal annealings. This diffusion through nanopipes is detrimental to the electrical characteristics of Ni-InGaN/GaN Schottky barriers. The use of an HP GaN buffer layer effectively reduced the nanopipe and surface micromesa densities. However, in order to further improve the electrical characteristics of the InGaN/GaN material, methods for further reducing or terminating surface micromesas on the surface (e.g., with thin surface dielectrics) are needed.

ACKNOWLEDGMENTS

This work was supported in part by the University of California at San Diego Center for Wireless Communications, by the FutureWei Technologies Inc., by National Science Foundation grant of NSF-ECCS-901113, and by the UC Discovery Grant Program.

[1]S. Nakamura, M. Senoh, and T. Mukai, Appl. Phys. Lett. **62**, 2390 (1993).
[2]T. Mukai, M. Yamada, and S. Nakamura, Jpn. J. Appl. Phys. **38**, 3976 (1999).
[3]T. Makimoto, K. Kumakura, and N. Kobayashi, Appl. Phys. Lett. **83**, 1035 (2003).
[4]S. N. Mohammad and H. Morkoc, J. Appl. Phys. **78**, 4200 (1995).
[5]W. Lu, L. Wang, S. Gu, D. P. R. Aplin, D. M. Estrada, P. K. L. Yu, and P. M. Asbeck, IEEE Electron Device Lett. **31**, 1119 (2010).
[6]W. Lu, L. Wang, S. Gu, D. P. R. Aplin, P. K. L. Yu, and P. M. Asbeck, in IEEE 2011 International Symposium on Semiconductor Device Research (ISDRS), College Park, MD, 7-9 December, 2011.

[7]X. H. Wu, L. M. Brown, D. Kapolnek, S. Keller, B. Keller, S. P. DenBaars, and J. S. Speck, J. Appl. Phys. **80**, 3228 (1996).
[8]W. Qian, M. Skowronski, K. Doverspike, L. B. Rowland, and D. K. Gaskill, J. Cryst. Growth **151**, 396 (1995).
[9]W. Qian, G. S. Rohrer, M. Skowronski, K. Doverspike, L. B. Rowland, and D. K. Gaskill, Appl. Phys. Lett. **67**, 2284 (1995).
[10]F. C. Frank, Acta Crystallogr. **4**, 497 (1951).
[11]H. Tanaka, Y. Uemura, and Y. Inomata, J. Cryst. Growth **53**, 630 (1981).
[12]H. M. Hobgood, D. L. Barrett, J. P. Mchugh, R. C. Clarke, S. Sriram, A. A. Burk, J. Greggi, C. D. Brandt, R. H. Hopkins, and W. J. Choyke, J. Cryst. Growth **137**, 181 (1994).
[13]P. G. Neudeck and J. A. Powell, IEEE Electron Device Lett. **15**, 63 (1994).
[14]P. G. Neudeck and C. Fazi, IEEE Electron Device Lett. **18**, 96 (1997).
[15]S. K. Hong, B. J. Kim, H. S. Park, Y. Park, S. Y. Yoon, and Y. I. Kim, J. Cryst. Growth **191**, 275 (1998).
[16]Y. Ono, Y. Iyechika, T. Takada, K. Inui, and T. Matsue, J. Cryst. Growth **189**, 133 (1998).
[17]K. Matsumoto and A. Tachibana, J. Cryst. Growth **272**, 360 (2004).
[18]W. Lu, L. Wang, S. Gu, D. P. R. Aplin, D. M. Estrada, P. K. L. Yu, and P. M. Asbeck, IEEE Trans. Electron Device **58**, 1986 (2011).
[19]S. Nakamura, Jpn. J. Appl. Phys. **30**, L1705 (1991).
[20]B. Heying, X. H. Wu, S. Keller, Y. Li, D. Kapolnek, B. P. Keller, S. P. DenBaars, and J. S. Speck, Appl. Phys. Lett. **68**, 643 (1996).
[21]J. C. Zhang, D. G. Zhao, J. F. Wang, Y. T. Wang, J. Chen, J. P. Liu, and H. Yang, J. Cryst. Growth **268**, 24 (2004).
[22]A. Zubrilov, *Properties of Advanced Semiconductor Materials: GaN, AIN, InN, BN, SiC, SiGe* (John Wiley & Sons, Inc., New York, 2001).
[23]N. Ohtani, M. Katsuno, T. Fujimoto, T. Aigo, and H. Yashiro, J. Cryst. Growth **226**, 254 (2001).
[24]X. Xu, R. P. Vaudo, J. Flynn, and G. R. Brandes, J. Electron Mater. **31**, 402 (2002).
[25]S. K. Hong, T. Yao, B. J. Kim, S. Y. Yoon, and T. I. Kim, Appl. Phys. Lett. **77**, 82 (2000).
[26]X. H. Wu, C. R. Elsass, A. Abare, M. Mack, S. Keller, P. M. Petroff, S. P. DenBaars, J. S. Speck, and S. J. Rosner, Appl. Phys. Lett. **72**, 692 (1998).
[27]Z. L. Miao, T. J. Yu, F. J. Xu, J. Song, C. C. Huang, X. Q. Wang, Z. J. Yang, G. Y. Zhang, X. P. Zhang, D. P. Yu, and B. Shen, Appl. Phys. Lett. **95**, 231909 (2009).
[28]T. Kehagias, G. P. Dimitrakopulos, J. Kioseoglou, H. Kirmse, C. Giesen, M. Heuken, A. Georgakilas, W. Neumann, T. Karakostas, and P. Komninou, Appl. Phys. Lett. **95**, 071905 (2009).
[29]H. K. Cho, J. Y. Lee, G. M. Yang, and C. S. Kim, Appl. Phys. Lett. **79**, 215 (2001).
[30]H. Zhang, E. J. Miller, E. T. Yu, C. Poblenz, and J. S. Speck, Appl. Phys. Lett. **84**, 4644 (2004).
[31]J. K. Sheu and G. C. Chi, J. Phys.: Condens. Matter **14**, R657 (2002).
[32]C. Y. Hsu, W. H. Lan, and Y. S. Wu, Appl. Phys. Lett. **83**, 2447 (2003).